Crystal Structures and Magnetic Properties of d-pπ Organic Conductors, $(EDT\text{-}TTF)_4CoCl_4(1,1,2\text{-}TCE)_x$ and Related Materials

Hatsumi Mori,* Naoki Sakurai, Shoji Tanaka, and Hiroshi Moriyama*,†

International Superconductivity Technology Center, Shinonome, Koto-ku, Tokyo 135-0062

†Department of Chemistry, Faculty of Science, Toho University, Miyama, Chiba 274-8510

(Received November 9, 1998)

A new series of d-pπ organic conductors ($(EDT\text{-}TTF)_4CoX_4(solvent)_x$ [EDT-TTF = ethylenedithiotetrathiafulvalene; X = Cl, Br; solvent = 1,1,2-TCE(trichloroethane), CH_2Cl_2]) consists of anions including 3d localized spins and donors containing itinerant pπ electrons. The crystal and band structure analyses show that these salts have face-to-face regular donor stacking, the so-called β-type donor arrangement, and that the calculated Fermi surfaces are closed due to relatively large interchain interactions. Resistivity measurements show the metallic behaviors down to 80 K [$(EDT\text{-}TTF)_4CoCl_4(1,1,2\text{-}TCE)_x$], 235 K [$(EDT\text{-}TTF)_4CoCl_4(CH_2Cl_2)_x$], 110 K [$(EDT\text{-}TTF)_4CoBr_4(1,1,2\text{-}TCE)_x$], and 190 K [$(EDT\text{-}TTF)_4CoBr_4(CH_2Cl_2)_x$], respectively. Especially, for $(EDT\text{-}TTF)_4CoCl_4(1,1,2\text{-}TCE)_x$, the ESR measurements indicate that the linewidth attributed to $EDT\text{-}TTF^+$ increases and that the g-value decreases rapidly when the resistivity starts increasing below 80 K, owing to substantially the dipole–dipole interaction between pπ ($EDT\text{-}TTF^+$)-3d (Co^{2+}) spins. At around 33 and 20 K, the anomalies of the ESR linewidth have been observed, suggesting the instability of the pπ part.

Recently, the d(f)-π system has been extensively investigated in order to obtain a new electronic state with a d(f)-π interaction. There is, however, only a slight magnetic exchange interaction for most d-pπ systems, where the itinerant pπ spins in a donor layer and localized 3d spins in a counter anion sheet coexist. It is recognized that the distance between d-pπ spins and the magnetism of pπ spins are important to give birth to magnetic interactions in a d-pπ system.

The rare cases which have curious electronic states due to d-pπ magnetic interactions are the following: (1) The antiferromagnetism of $3d^5$ spins on Fe^{3+} ($S = 5/2$) induces a metal-insulator transition at 8 K for λ-$(BETS)_2FeCl_4$ [BETS = bis(ethylenedithio)tetraselenafulvalene], while an isostructural salt without localized spins, λ-$(BETS)_2GaCl_4$, affords superconductivity.[1] The short distance between $BETS^+$ and $FeCl_4^-$ and the strong correlation of a donor part, $BETS^+$, are the important factors for the antiferromagnetic order of spins on Fe^{3+}. (2) The mixture of a pπ band of DCNQI (DCNQI = *N*,*N*′-dicyano-*p*-benzoquinone diimine) and a 3d band of Cu for $(DCNQI)_2Cu$ gives a variety of physical properties, not only at an ambient pressure, but also under a pressurized condition.[2] The electronic state is determined by the degree of hybridization of the pπ-3d orbitals. When the magic number of $Cu^{+4/3}$ and $DCNQI^{-2/3}$ was obtained, a three-fold lattice instability occurred and charge ordering, like Cu^+, Cu^+, and Cu^{2+}, could be observed. (3) The antiferromagnetic order of 3d spins through a pπ system has been obtained in $(BEDT\text{-}TTF)_3CuBr_4$ [T_N = 7.65 K],[3] $[Ni(dddt)_2]_3FeBr_4$ [T_N = 6 K] (dddt = 5,6-dihydro-1,4-dithiin-2,3-dithiolate),[4] and (TMTSF)$FeCl_4$ [T_N = 4 K] (TMTSF = tetramethyltetraselenafulvalene).[5] For $(BEDT\text{-}TTF)_3CuBr_4$, the Weiss temperature of the sum of the localized pπ spins on $BEDT\text{-}TTF^+$ and 3d spins on Cu^{2+} is −100 K; also after the disappearance of spins on donors at 59 K, the antiferromagnetic order of 3d spins through singlet pπ orbitals is obtained at 7.65 K. It is also curious that (TMTSF)$FeCl_4$ has a magnetic order at 4 K, even when the nonmagnetic singlet state is observed in the donor part.

In this work, a series of EDT-TTF salts containing magnetic anions was investigated. Usually EDT-TTF salts are low dimensional and the ground states are nonmagnetic insulators,[6—9] except for an antiferromagnet, $(EDT\text{-}TTF)_4Cu_2Br_6$,[10] owing to strongly dimerized donors. In expectation of a new electronic state by an interaction between a low-dimensional instability of the pπ part and the magnetism of localized 3d spins, a series of $(EDT\text{-}TTF)_4CoX_4(solvent)_x$ [X = Cl, Br; solvent = 1,1,2-TCE, CH_2Cl_2] was newly prepared. Crystal and electronic structure analyses as well as electrical resistivity, magnetic susceptibility, and ESR measurements were studied in this work in order to investigate the interaction between d-pπ electrons.

Experimental

Single crystals were prepared by an electrocrystallization method using $[(n\text{-}C_4H_9)_4N]_2\cdot CoX_4$ (X = Cl, Br) as the electrolytes in 1,1,2-TCE or CH_2Cl_2 at a constant current of 0.5 μA. The preparation conditions, stoichiometries, and electrical conductivities of EDT-TTF salts are given in Table 1, and the crystallographic data, atomic coordinates, and intramolecular bond lengths and angles are listed in Tables 2, 3, and 4, respectively. Crystal data were collected

Table 1. Preparation Conditions, Stoichiometries, and Electrical Conductivities of EDT-TTF Salts

Preparation electrolyte[a]	Solvent[b]	Complexes[c]	Electrical conductivity
$TBA_2{\cdot}CoCl_4$	TCE	$EDT_4CoCl_4(TCE)_x$[d]	$\sigma_{RT} = 10\ S\ cm^{-1}$, $T_{MI} = 80$ K, $E_a = 0.007$ eV
$TBA_2{\cdot}CoCl_4$	CH_2Cl_2	$EDT_4CoCl_4(CH_2Cl_2)_x$[e]	$\sigma_{RT} = 34\ S\ cm^{-1}$, $T_{MI} = 235$ K, $E_a = 0.011$ eV
$TBA_2{\cdot}CoBr_4$	TCE	$EDT_4CoBr_4(TCE)_x$[d]	$\sigma_{RT} = 78\ S\ cm^{-1}$, $T_{MI} = 110$ K, $E_a = 0.006$ eV
$TBA_2{\cdot}CoBr_4$	CH_2Cl_2	$EDT_4CoBr_4(CH_2Cl_2)_x$[d]	$\sigma_{RT} = 1\ S\ cm^{-1}$, $T_{MI} = 190$ K

a) TBA = $[(n\text{-}C_4H_9)_4N]$. b) TCE = 1,1,2-trichloroethane. c) EDT = EDT-TTF. d) The stoichiometry is determined by the EDX measurement and the crystal structure analysis. e) The stoichiometry is determined by EDX measurement.

Table 2. Crystallographic Data of EDT-TTF Salts [EDT = EDT-TTF; TCE = 1,1,2-Trichloroethane]

	$EDT_4CoCl_4(TCE)_x$	$EDT_4CoBr_4(TCE)_x$	$EDT_4CoBr_4(CH_2Cl_2)_x$
Chemical formula ($x = 1$)	$CoCl_7S_{24}C_{34}H_{27}$	$CoBr_4Cl_3S_{24}C_{34}H_{27}$	$CoBr_4Cl_2S_{24}C_{33}H_{26}$
FW ($x = 1$)	1512.3	1690.1	1641.6
System	Monoclinic	Monoclinic	Monoclinic
Space group	$C2/m$ (#12)	$C2/m$ (#12)	$C2/m$ (#12)
a/Å	12.864(4)	12.97(1)	13.037(6)
b/Å	31.846(6)	32.544(8)	32.393(7)
c/Å	7.091(5)	7.10(1)	7.103(5)
α/°	90	90	90
β/°	108.55(3)	108.97(7)	108.92(4)
γ/°	90	90	90
V/Å^3	2753(1)	2834(4)	2837(2)
Z	2	2	2
R	0.082	0.083	0.085
D_c	1.82	1.98	1.92
No. of ref.	571	553	1030
	$\|I_0\| > 5\sigma\|I_0\|$	$\|I_0\| > 3\sigma\|I_0\|$	$\|I_0\| > 3\sigma\|I_0\|$
$2\theta_{max}$/°	60	60	60
λ/Å	0.71073	0.71073	0.71073

by a Rigaku AFC5R diffractometer. The crystal structures were solved by a direct method (Shelxs 86[11]) and refined by a least-squares procedure. Anisotropic thermal parameters were adapted for all non-hydrogen atoms. The atomic coordinates of (EDT-TTF)$_4$CoBr$_4$(1,1,2-TCE)$_x$ and (EDT-TTF)$_4$CoBr$_4$(CH$_2$Cl$_2$)$_x$ and complete $F_o - F_c$ data of (EDT-TTF)$_4$CoCl$_4$(1,1,2-TCE)$_x$, (EDT-TTF)$_4$CoBr$_4$(1,1,2-TCE)$_x$, and (EDT-TTF)$_4$CoBr$_4$(CH$_2$Cl$_2$)$_x$ are deposited as Document No. 72013 at the Office of the Editor of Bull. Chem. Soc. Jpn.

The electrical resistivity was measured by a conventional four-probe method. Gold wires (Tanaka Kikinzoku, 18 $\mu m\phi$) were attached to a crystal with gold paste (Tokuriki Chemicals, No. 8560) as electrodes. The ESR measurements were carried out from 5 to 300 K with utilizing a JEOL JES-RE3X (9.2 GHz, X-band) spectrometer equipped with an Air Product and Chemicals inc. LTR-3 cryostat and a Scientific Instrument model 5500 temperature controller. The temperature was controlled and monitored with AuFe-chromel thermocouples. DPPH (g = 2.0034) was used as a standard. The magnetic susceptibility was measured by a SQUID magnetometer (Quantum Design Model MPMS7) by applying a magnetic field of 0.2—5 T. The spin susceptibility was estimated by subtracting the core contribution of components using Pascal's law.[12]

Results and Discussion

Figure 1 shows the crystal structure of (EDT-TTF)$_4$CoCl$_4$(1,1,2-TCE)$_x$. An EDT-TTF molecule is on a two-fold axis and a $CoCl_4$ is on a mirror plane. Because of the positional disorder of $CoCl_4$, two possible sites are illustrated in Fig. 1(a), and the occupancy is 0.5. As a result, two EDT-TTF molecules and 1/2 of the $CoCl_4$ anion are crystallographically independent. The included solvent, 1,1,2-TCE, is strongly disordered and located at the vacant place of a disordered $CoCl_4$ anion. The occupancy of the solvent was calculated from the remaining Fourier peak [Cl(11),Cl(12), Cl(13) in Table 3] to be x = 1.06. As shown in Fig. 1, a donor layer and an anion sheet stack along the b-axis. In a donor sheet, donors stack regularly along the c-axis in a manner of the usual head-to-tail configuration with an interplaner spacing of donors of 3.56 Å (Fig. 1(b)). The face-to-face donor arrangement is called β-type, which is commonly seen in EDT-TTF salts. Strictly speaking, our salts, (EDT-TTF)$_4$CoCl$_4$(TCE)$_x$, and (EDT-TTF)$_2$X [X = $AuBr_2$,[7] AuI_2[8]], afford *regular* donor stacking, whereas (EDT-TTF)$_2$X [X = $Au(CN)_4$,[6] BF_4,[6] ClO_4,[6] ReO_4,[6] PF_6,[6] TaF_6,[6] AsF_6,[6] $GaCl_4$,[9] $FeCl_4$[9]] have a *dimerized* donor arrangement like β-(BEDT-TTF)$_2$X [X = I_3,[13a] AuI_2,[13b] IBr_2[13c]]. The terminal C(1) and C(11) atoms in the ethylenedithio-fragment are about 0.44 and 0.34 Å out of a TTF plane, as usually observed in BEDT-TTF salts.

In order to investigate the electronic structure of (EDT-TTF)$_4$CoCl$_4$(1,1,2-TCE)$_x$, the overlap integrals between two HOMO's (EDT-TTF) were calculated by an extended

Table 3. Atomic Coordinates and Equivalent Isotropic Thermal Parameters of (EDT-TTF)$_4$CoCl$_4$ (1,1,2-TCE)$_x$

Atom	x	y	z	B_{eq} [a)]
Co(1)	0.250(1)	0.0000	0.915(3)	3.7(5)
Cl(1)	0.436(2)	0.0000	0.993(5)	3.3(8)
Cl(2)	0.205(3)	0.0000	1.191(5)	4.3(10)
Cl(3)	0.182(2)	0.0565(7)	0.738(4)	7.1(9)
Cl(11)	0.872(5)	0.0000	0.395(9)	11(2)
Cl(12)	0.832(5)	0.0000	0.674(8)	8(2)
Cl(13)	0.816(2)	0.0596(7)	0.260(4)	5.7(9)
S(1)	0.1442(9)	0.4000(4)	0.580(2)	4.9(3)
S(3)	0.1214(8)	0.3095(3)	0.571(2)	2.8(3)
S(5)	0.1182(8)	0.2080(3)	0.575(2)	2.7(3)
S(11)	0.1441(9)	0.1446(3)	0.086(2)	3.8(3)
S(13)	0.1199(8)	0.2361(3)	0.067(2)	3.7(3)
S(15)	0.1187(9)	0.3371(3)	0.065(2)	3.6(3)
C(1)	0.050(3)	0.443(1)	0.460(6)	4(1)
C(3)	0.056(2)	0.359(1)	0.542(6)	2(1)
C(5)	0.0000	0.279(1)	0.5000	1(1)
C(6)	0.0000	0.234(1)	0.5000	1(1)
C(7)	0.058(3)	0.159(1)	0.541(7)	4(1)
C(11)	0.048(2)	0.101(1)	0.077(5)	2.1(10)
C(13)	0.054(2)	0.186(1)	0.026(6)	3(1)
C(15)	0.0000	0.269(2)	0.0000	3(1)
C(16)	0.0000	0.308(2)	0.0000	1(1)
C(17)	0.051(3)	0.386(1)	0.034(8)	5(1)

a) $B_{eq} = 4/3(\sum_i \sum_j B_{ij} \boldsymbol{a}_i \cdot \boldsymbol{a}_j)$.

Hückel method, and the band structure was obtained by the tight binding approximation using the calculated overlap integrals.[14] The estimated overlap integrals are listed in Table 5. The intrachain interaction is the largest and the anisotropy in the conduction plane of (EDT-TTF)$_4$CoCl$_4$(1,1,2-TCE)$_x$, Sc/Sa, is 3.5, which is relatively small among EDT-TTF salts. The calculated Fermi surface of this salt is closed, although other EDT-TTF salts have waved open Fermi surfaces.[6–9]

Up to now, we have prepared not only (EDT-TTF)$_4$CoCl$_4$(1,1,2-TCE)$_x$, but also related materials: (EDT-TTF)$_4$CoBr$_4$(1,1,2-TCE)$_x$, (EDT-TTF)$_4$CoBr$_4$(CH$_2$Cl$_2$)$_x$, (EDT-TTF)$_4$CoCl$_4$(CH$_2$Cl$_2$)$_x$, (EDT-TTF)$_3$MnCl$_4$,[15] and (EDT-TTF)$_3$ZnCl$_4$.[15] The crystallographic data of (EDT-TTF)$_4$CoBr$_4$(1,1,2-TCE)$_x$ and (EDT-TTF)$_4$CoBr$_4$(CH$_2$Cl$_2$)$_x$ are listed in Table 2. They are isostructural to (EDT-TTF)$_4$CoCl$_4$(1,1,2-TCE)$_x$. The calculated overlap integrals and the band structure are given in Table 5 and Figs. 2(b) and 2(c), respectively. Owing to the relatively large interchain interactions of related materials, the calculated Fermi surfaces are closed with slightly different anisotropies. Since (EDT-TTF)$_4$CoCl$_4$(CH$_2$Cl$_2$)$_x$, (EDT-TTF)$_3$MnCl$_4$, and (EDT-TTF)$_3$ZnCl$_4$ have substantially poor crystal qualities, crystal structure analyses are being performed.

The electrical resistivities of four CoX$_4$ salts are shown in Fig. 3. Because these CoX$_4$ salts contain solvents, freshly prepared crystals were used for these electrical resistivity measurements. The electrical conductivity of (EDT-TTF)$_4$CoCl$_4$(1,1,2-TCE)$_x$ at room temperature is 10 S cm^{-1}, and the weak metallic behavior remains down to 80 K. Below this temperature, the resistivity gradually increases, and the activation energy is 0.007 eV. Other CoX$_4$ salts have similar behaviors as (EDT-TTF)$_4$CoCl$_4$(1,1,2-TCE)$_x$. The room temperature conductivities are 34, 78, and 1 S cm^{-1} and metallic down to 235, 110, and 190 K for (EDT-TTF)$_4$CoCl$_4$(CH$_2$Cl$_2$)$_x$, (EDT-TTF)$_4$CoBr$_4$(1,1,2-TCE)$_x$, and (EDT-TTF)$_4$CoBr$_4$(CH$_2$Cl$_2$)$_x$, respectively.

Table 4. Intramolecular Bond Lengths (Å) and Angles (degree) of (EDT-TTF)$_4$CoX$_4$(solvent)$_x$ [X = Cl, Br; solvent = 1, 1, 2-TCE, CH$_2$Cl$_2$; abbreviated as CoX$_4$(solvent)$_x$]

	CoCl$_4$(TCE)$_x$	CoBr$_4$(TCE)$_x$	CoBr$_4$(CH$_2$Cl$_2$)$_x$
Co–X1	2.28(3)	2.36(2)	2.445(9)
Co–X2	2.22(4)	2.31(3)	2.50(1)
Co–X3	2.21(2)	2.50(1)	2.402(6)
S1–C1	1.85(4)	1.82(5)	1.80(2)
S1–C3	1.69(3)	1.75(4)	1.67(2)
S3–C3	1.77(3)	1.75(4)	1.80(2)
S3–C5	1.77(3)	1.76(3)	1.73(1)
S5–C6	1.66(3)	1.71(3)	1.73(2)
S5–C7	1.73(4)	1.74(4)	1.75(2)
C1–C1[a)]	1.57(9)	1.5(1)	1.52(4)
C3–C3[a)]	1.37(6)	1.32(7)	1.36(3)
C5–C6	1.44(7)	1.33(8)	1.34(4)
C7–C7[a)]	1.42(7)	1.32(7)	1.29(3)
S11–C11	1.84(4)	1.82(4)	1.84(2)
S11–C13	1.71(3)	1.67(4)	1.75(2)
S13–C13	1.79(3)	1.76(4)	1.76(2)
S13–C15	1.80(3)	1.75(3)	1.74(2)
S15–C16	1.72(3)	1.70(3)	1.75(1)
S15–C17	1.77(4)	1.71(4)	1.74(2)
C11–C11[b)]	1.37(5)	1.52(6)	1.61(3)
C13–C13[b)]	1.33(6)	1.47(7)	1.31(3)
C15–C16	1.24(7)	1.38(7)	1.29(4)
C17–C17[b)]	1.23(7)	1.25(7)	1.32(4)
X1–Co–X2	113(1)	111(1)	111.5(4)
X2–Co–X3	109(1)	110.2(8)	106.4(3)
X3–Co–X1	109.8(9)	109.8(8)	107.9(3)

Symmetry transformations used to generate equivalent atoms: a) $-x, y, 1-z$. b) $-x, y, -z$.

In order to observe the magnetic properties, the magnetic susceptibility of (EDT-TTF)$_4$CoCl$_4$(1,1,2-TCE)$_x$ was measured from 300 to 2 K. The magnetic susceptibility (χ_{TOTAL}) at room temperature is 1.18×10^{-2} emu mol^{-1}, which consists of localized 3d (Co^{2+}; $S = 3/2$) and itinerant pπ parts. Since the spin susceptibility at room temperature of metallic organic materials is on the order of 10^{-4} emu mol^{-1}, as observed in $\varkappa$-(BEDT-TTF)$_2$Cu(NCS)$_2$ (4.2×10^{-4} emu mol^{-1}),[16] θ-(BEDT-TTF)$_2$CsZn(SCN)$_4$ (3.3×10^{-4}),[17a] and θ-(BEDT-TTF)$_2$RbZn(SCN)$_4$ (6.0×10^{-4}),[17a] the susceptibility of the pπ part is two orders smaller than that of the total magnetic susceptibility, 1.18×10^{-2} emu mol^{-1}. Figure 4 shows the temperature dependence of the reciprocal magnetic susceptibility (χ^{-1}) and χT. The susceptibility attributed to mainly 3d spins on Co^{2+} follows the Curie–Weiss law from 300 to 40 K with the Curie

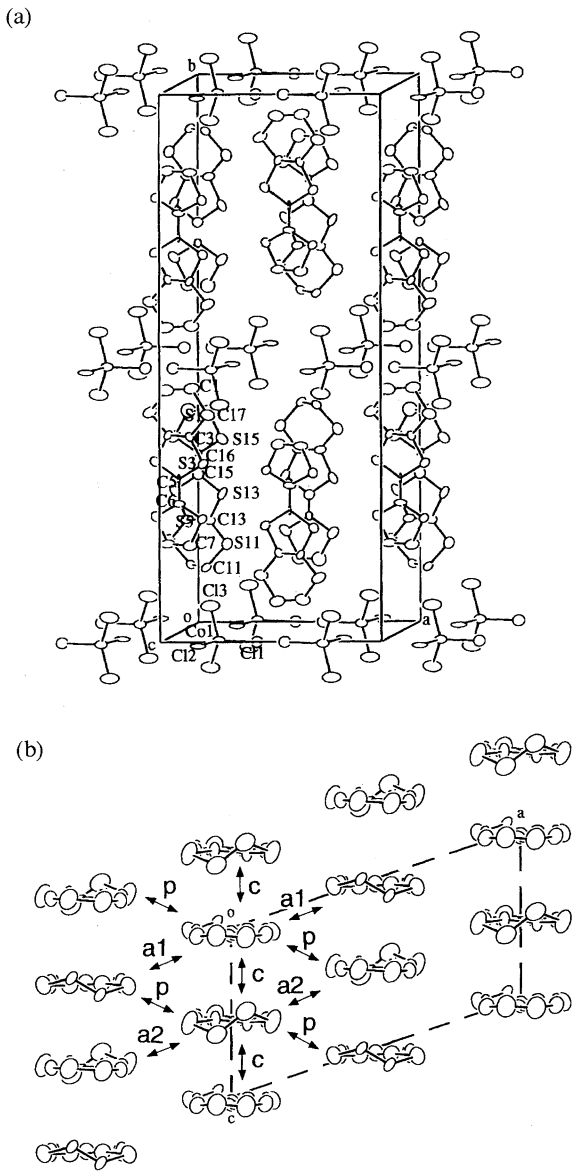

Fig. 1. (a) Crystal structure and (b) donor arrangement of $(EDT\text{-}TTF)_4CoCl_4(1,1,2\text{-}TCE)_x$.

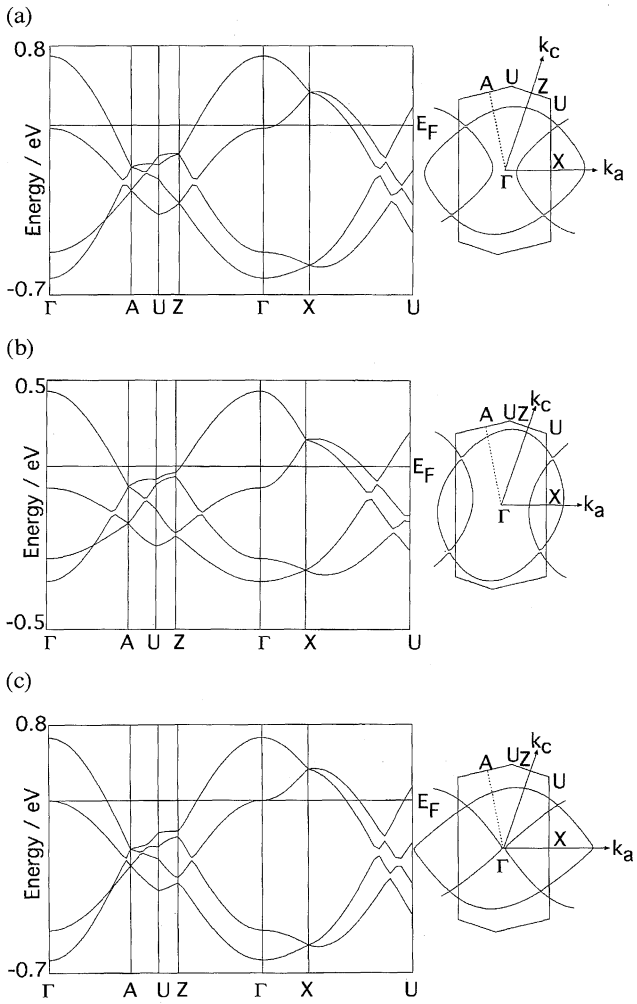

Fig. 2. Band structure of (a) $(EDT\text{-}TTF)_4CoCl_4(1,1,2\text{-}TCE)_x$, (b) $(EDT\text{-}TTF)_4CoBr_4(CH_2Cl_2)_x$, and (c) $(EDT\text{-}TTF)_4CoBr_4(1,1,2\text{-}TCE)_x$.

constant (C = 3.55 emu K mol^{-1}) and the Weiss temperature (θ = −6 K). When we assume $S = 3/2$ and $g = 2.75$ from C = 3.55 emu K mol^{-1}, the estimated spin density of $(EDT\text{-}TTF)_4CoCl_4(1,1,2\text{-}TCE)_x$ is 1 spin/formula. The θ-value (−6 K), indicates a small antiferromagnetic interaction between 3d spins through pπ spins. The rapid decrease of χT at low temperature can be explained by the fact that the crystal field around Co^{2+} produces zero field splitting at around 10 K between Kramers' doublets, Ms = ±3/2 and ±1/2 orbitals. As a result, the state population depending upon the Boltzmann principle induces a decrease in χT upon lowering the temperature.[17b,17c]

The behaviors of the itinerant spins on $EDT\text{-}TTF^+$ and the localized ones on Co^{2+} can be investigated independently by an ESR measurement. At 280 K, one Lorentzian signal attributed to $EDT\text{-}TTF^+$ was observed, and below 50 K the broad signals of Co^{2+} spins were superimposed

Table 5. Overlap Integrals ($\times 10^{-3}$) of $(EDT\text{-}TTF)_4CoX_4(solvent)_x$ [X = Cl, Br; solvent = 1,1,2-TCE, CH_2Cl_2]

Overlap integrals	$EDT_4CoCl_4(TCE)_x$[a)]	$EDT_4CoBr_4(TCE)_x$[a)]	$EDT_4CoBr_4(CH_2Cl_2)_x$[a)]
c	−26.1	−26.6	−13.1
a1	7.5	7.9	5.6
a2	7.3	6.1	6.4
p	3.5	2.5	3.7

a) EDT = EDT-TTF.

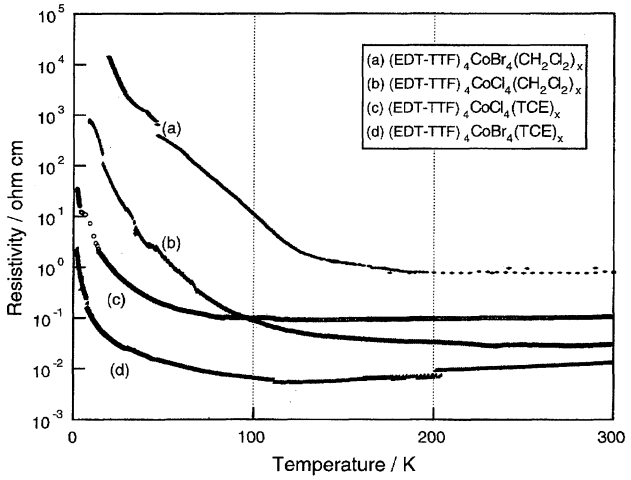

Fig. 3. Temperature dependence of electrical resistivity of $(EDT\text{-}TTF)_4CoX_4(solvent)_x$ [X = Cl, Br; solvent = 1,1,2-TCE, CH_2Cl_2].

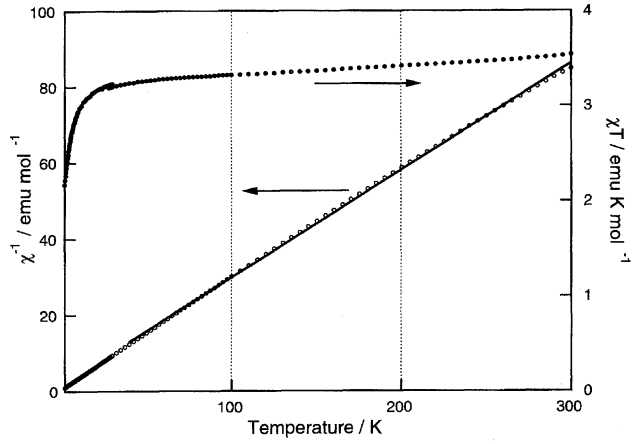

Fig. 4. Temperature dependence of magnetic susceptibility of $(EDT\text{-}TTF)_4CoCl_4(1,1,2\text{-}TCE)_x$. The solid line indicates the calculated Curie–Weiss plot (C = 3.55 emu mol K^{-1} and θ = −6 K).

(Fig. 5(a)). The angular dependence of signals at 5 K is shown in Fig. 5(b). Since Co^{2+} and $EDT\text{-}TTF^+$ signals behave independently, the magnetic exchange interaction between d-pπ spins is small. The temperature dependences of the ESR signal intensity, linewidth, and g-value of $EDT\text{-}TTF^+$ are shown in Fig. 6. The g-value decreases rapidly upon applying a magnetic field along both the b^* and a^* axes below 80 K, corresponding to the metal-semiconductor transformation temperature. The g-shift does not substantially originate from the spin–spin interaction, since the signals of $EDT\text{-}TTF^+$ and Co^{2+} behave independently and the g-value of $EDT\text{-}TTF^+$ does not shift closer to that of Co^{2+}, but decreases with lowering temperature. The g-shift can be rewritten based on the shift of a resonant magnetic field from that at room temperature. As shown in Fig. 7(a), the temperature dependence of the inverse resonant magnetic field shift of $EDT\text{-}TTF^+$ (ΔH_{res}^{-1}), is almost linear, which indicates a Curie–Weiss behavior. Therefore, the decrease in the g-value of a $EDT\text{-}TTF^+$ signal below 80 K is not caused only by the magnetic order of $EDT\text{-}TTF^+$, but is also due to the local

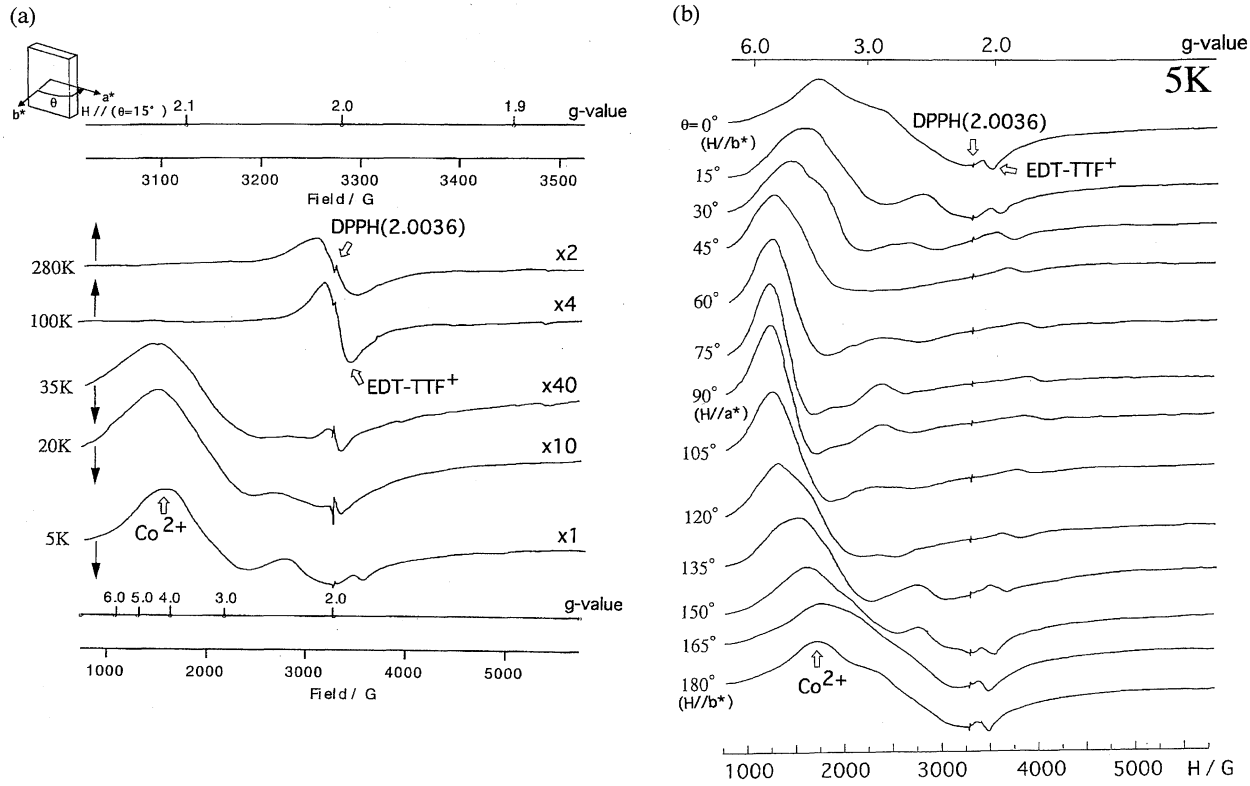

Fig. 5. (a) Temperature dependence and (b) angular dependence of ESR signals for $(EDT\text{-}TTF)_4CoCl_4(1,1,2\text{-}TCE)_x$. The static field is rotated along the $b^*(\theta = 0°)$–$a^*(\theta = 90°)$ plane.

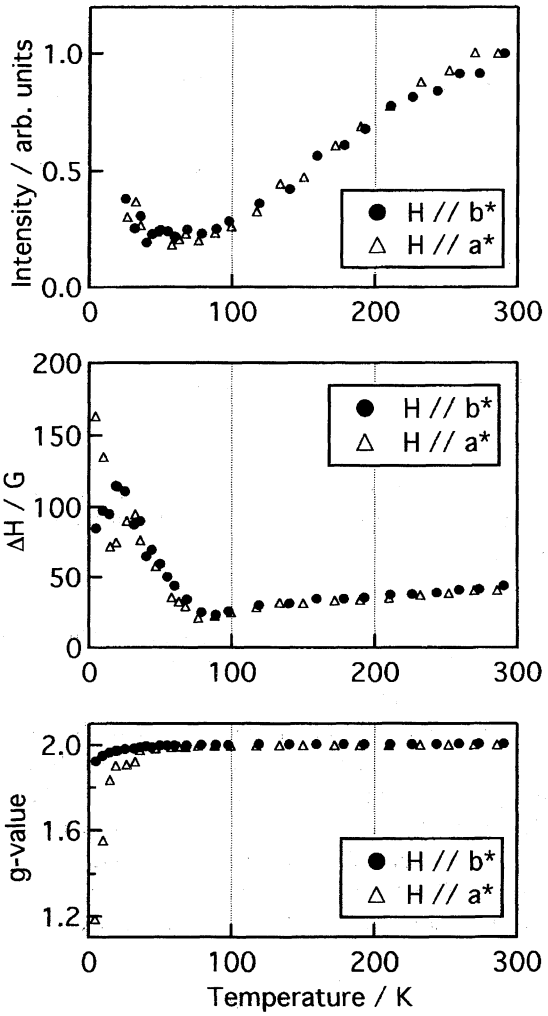

Fig. 6. Temperature dependence of ESR signal intensity, linewidth, and g-value of EDT-TTF$^+$ for (EDT-TTF)$_4$CoCl$_4$(1,1,2-TCE)$_x$.

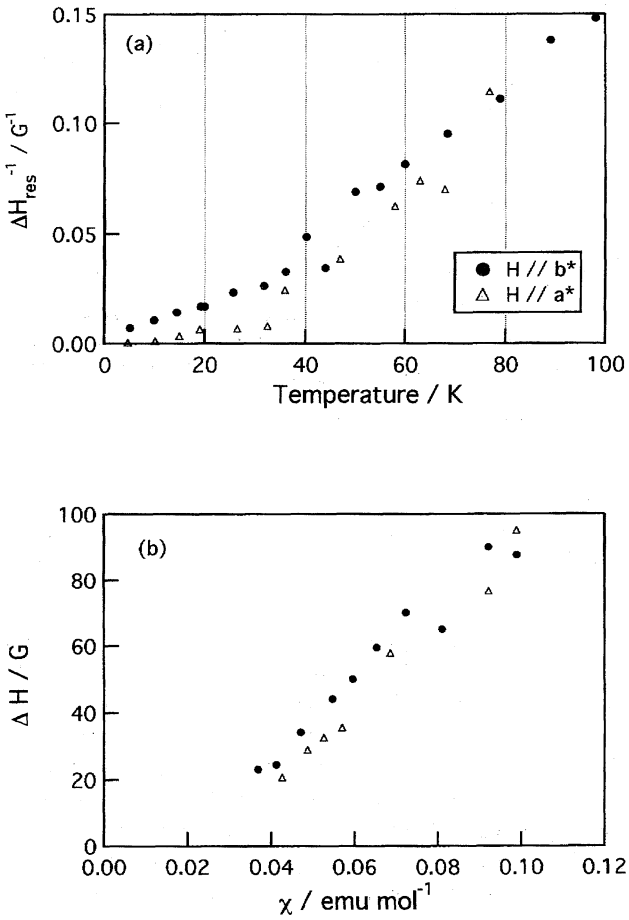

Fig. 7. (a) Temperature dependence of reciprocal value of the shift of resonant magnetic field (ΔH_{res}^{-1}) and (b) plot of ESR linewidth (ΔH) vs. magnetic susceptibility (χ) by SQUID measurement for (EDT-TTF)$_4$CoCl$_4$(1,1,2-TCE)$_x$.

magnetic field on EDT-TTF$^+$ spins produced by the magnetic moment of Co^{2+} spins, the so-called dipole–dipole interaction of pπ-3d spins. The g-shift of EDT-TTF$^+$ due to the dipole interaction with Co^{2+}, however, should be anisotropic. When a magnetic field is applied parallel to the two-dimensional sheet, a large magnetization of Co^{2+} induces a diamagnetic field to the EDT-TTF$^+$ layer. Then, the signal of EDT-TTF$^+$ shifts to a higher field, which means a decrease in the g-value. It is in good agreement with the rapid decrease of the g-values along the b^*-axis at low temperatures. On the other hand, the magnetic field perpendicular to the plane induces an internal magnetic field to both the anion and donor layers. Since the total applied field in the donor layer is higher than the external field, the g-value should shift "positive". The g-value along the b^*-axis, however, decrease slowly with lowering temperature. Then, although the g-shift can be explained mainly by the dipole–dipole interaction, the possibility of other effects remains. As for the ESR linewidth, the value at room temperature is 44 G ($H//b^*$) and 41 G ($H//a^*$), respectively, and decreases slightly down to 80 K. Below this temperature, it increases rapidly with anomalies at 20 K ($H//b^*$) and 33 K and 20 K ($H//a^*$), respectively. In order to investigate the effect of the local field of Co^{2+}, a plot of the ESR linewidth versus the magnetic susceptibility by the SQUID measurement between 80 and 33 K is given in Fig. 7(b). The linear relationship suggests that the fluctuation of the local field on Co^{2+} makes the linewidth of EDT-TTF$^+$ broaden at low temperatures. Moreover, the anomalies of the linewidth at 20 and 33 K are not due to Co^{2+} spins, since the angular dependence shows that the signals originated from EDT-TTF$^+$, and that Co^{2+} behave independently. Then, the anomalies might be an instability of pπ spins.

In conclusion, a series of 3d-pπ organic conductors, (EDT-TTF)$_4$CoX$_4$(solvent)$_x$, [X = Cl, Br; solvent = 1,1,2-TCE, CH_2Cl_2], was newly prepared. Crystal structure analyses show that in an anion sheet, an anion, CoX_4^{2-}, and a solvent have a positional disorder, and that in a donor layer, the face-to-face regular donor stacking is observed, so-called β-type donor arrangement. Due to the relatively large interchain interaction, the closed Fermi surface was calculated. The resistivity measurements show metallic behaviors down to 80 K [(EDT-TTF)$_4$CoCl$_4$(1,1,2-TCE)$_x$], 235 K [(EDT-TTF)$_4$CoCl$_4$(CH_2Cl_2)$_x$], 110 K [(EDT-TTF)$_4$CoBr$_4$(1,1,2-TCE)$_x$], and 190 K [(EDT-TTF)$_4$CoBr$_4$(CH_2Cl_2)$_x$], respec-

tively, with activation energies (0.006—0.011 eV) below those temperatures. The magnetic susceptibility of (EDT-TTF)$_4$CoCl$_4$(1,1,2-TCE)$_x$ follows the Curie–Weiss law with $C = 3.55$ emu mol K^{-1} ($S = 3/2$, $g = 2.75$) and $\theta = -6$ K, indicating a weak magnetic exchange interaction between pπ and 3d spins. The ESR measurements show that the rapid increase in the linewidth and the decrease in the g-value of (EDT-TTF)$_4$CoCl$_4$(1,1,2-TCE)$_x$ below 80 K mainly originate from the dipole–dipole interaction between the 3d-pπ spins. The anomalies of the linewidth at 33 and 20 K might be caused by an instability of the pπ part.

This work was supported by New Energy and Industrial Technology Development Organization (NEDO).

References

1) H. Kobayashi, H. Tomita, T. Naito, A. Kobayashi, F. Sakai, T. Watanabe, and P. Cassoux, *J. Am. Chem. Soc.*, **118**, 368 (1996).

2) R. Kato, H. Kobayashi, and A. Kobayashi, *J. Am. Chem. Soc.*, **111**, 5224 (1989); T. Mori, H. Inokuchi, A. Kobayashi, R. Kato, and H. Kobayashi, *Phys. Rev. B*, **38**, 5913 (1988).

3) J. Yamaura, K. Suzuki, Y. Kaizu, T. Enoki, K. Murata, and G. Saito, *J. Phys. Soc. Jpn.*, **65**, 2645 (1996).

4) T. Enoki, J. Yamaura, and A. Miyazaki, *Bull. Chem. Soc. Jpn.*, **70**, 2005 (1997).

5) R. Kumai, A. Asamitsu, and Y. Tokura, *Chem. Lett.*, **1996**, 753.

6) R. Kato, H. Kobayashi, and A. Kobayashi, *Chem. Lett.*, **1989**, 781.

7) T. Mori and H. Inokuchi, *Solid State Commun.*, **70**, 823 (1989).

8) A. Hountas, A. Terzis, G. C. Papavassiliou, B. Hilti, M. Burkle, C. W. Meyer, and J. Zambounis, *Acta Crystallogs., Sect. C*, **C46**, 228 (1990).

9) T. Kondo, L. A. Kushch, H. Yamochi, and G. Saito, *Mat. Res. Soc. Symp. Proc.*, **488**, 921 (1998).

10) H. Mori, T. Mori, and S. Tanaka, *Synth. Met.*, **70**, 877 (1995); H. Mori et al., private communication.

11) G. M. Sheldrick, "Crystallographic Computing 3," Oxford University Press, Oxford (1985), pp. 175—189.

12) "Kagaku Binran, Kisohen II," ver. 3, Maruzen Press, II-508 (1989).

13) a) V. F. Kaminskii, T. G. Prokhorova, R. P. Shivaeva, and E. B. Yagubskii, *JETP Lett.*, **39**, 17 (1984); b) H. H. Wang, M. A. Beno, U. Geiser, M. A. Firestone, K. S. Webb, L. Nunez, G. W. Crabtree, K. D. Carlson, J. M. Williams, L. J. Azevedo, J. F. Kwack, and J. E. Schirber, *Inorg. Chem.*, **24**, 2465 (1985); c) J. M. Williams, H. H. Wang, M. A. Beno, T. J. Emge, L. M. Sowa, P. T. Copps, F. Behrozi, L. N. Hall, K. D. Carlson, and G. W. Crabtree, *Inorg. Chem.*, **23**, 3839 (1984).

14) T. Mori, A. Kobayashi, Y. Sasaki, H. Kobayashi, G. Saito, and H. Inokuchi, *Bull. Chem. Soc. Jpn.*, **57**, 627 (1984).

15) H. Mori et al., private communication.

16) K. Nozawa, T. Sugano, H. Urayama, H. Yamochi, G. Saito, and M. Kinoshita, *Chem. Lett.*, **1988**, 617.

17) a) H. Mori, S. Tanaka, and T. Mori, *Phys. Rev. B*, **57**, 12023 (1998); b) R. L. Carlin, "Magnetochemistry," Springer-Verlag, Berlin and Heidelberg (1986), p. 25; c) H. Mori, S. Tanaka, and T. Mori, *J. Phys. I, Fr.*, **6**, 1987 (1996).